International Journal of Energy
ISSN: 2957-9473 | Vol. 5, No. 3, 2024

Multiscale Fracture Rupture Characteristic Study and Application of Sichuan Shale During Hydraulic Fracturing

Xuewen Shi [1], Chao Zeng [2, *], Ruofeng Zhang [1], Chen Liu [2], Chen Yin [2], Dongjun Zhang [1], Caifu Xiong [2], Shanshi Wen [1]

[1] Shale Gas Development Research Institute of PetroChina Southwest Oil & Gas Field Company, Chengdu Sichuan, 610095, China
[2] School of Environment and Resource, Southwest University of Science and Technology, Mianyang Sichuan, 621010, China

*** Corresponding author:** Chao Zeng (Email: 1326629950@qq.com)

Abstract: Microseismic monitoring is a conventional technique used to evaluate the hydraulic fracturing effect according to the temporal and spatial distribution and evolution of located microseismic events (MEs) at the macroscale. It is generally thought that few or no located MEs reflects poor hydraulic fracturing results and that more located MEs indicate a better result, but the variability in rupture behavior at different rupture scales is ignored. This paper focuses on the characteristics of multiscale rupture of shale by combining laboratory acoustic emission and field microseismic monitoring. The results demonstrate that shear slippage along fractures mainly dominates the rupture behavior. If no pre-existing fracture is present at the microscale, in the laboratory experiment, a rupture mainly occurs along bedding planes, veins and cracks and predominantly slips, which can help develop a fracture network. Because seismic wave energy is related to the rupture scale and stronger MEs are generated by larger ruptures along pre-existing fractures, fault damage zones or isolated small faults, these slippages may cause casing deformation, and the connected fracture networks may result in fluid seepage. A large number of weak MEs are ignored during fracturing because too little energy is released from small ruptures to be effectively detected, but they usually indicate a fracture network and greatly contribute to gas production in the long term. Therefore, ruptures in shale generally occur from the microscale to macroscale and express similar rupture behavior at each scale but result in different seismic characteristics, located ME distributions, fracture evolutions and engineering effects.

Keywords: Microseismic Monitoring; Acoustic Emission; Unconventional Reservoir; Rupture Size; Hydraulic Fracturing.

1. Introduction

Hydraulic fracturing has been widely used in unconventional reservoirs such as shale, tight sand, and coal and in enhanced geothermal systems. During its sedimentary evolution and under tectonic stress, such rock produces pores, veins/bedding planes, cracks, pre-existing fractures, and faults. Some areas with large pre-existing fractures or small faults are also represented as fault damage zones because there are no clear boundaries between the larger fractures and small faults, as faults are often complex and form a damaged rock volume with many structures of different scales, orientations, intensities and densities under tectonic stress[1]. Such characteristics are represented as geological heterogeneity. The pre-existing fractures are important spaces for storing oil/gas and other fluids and act as the main seepage channels for fluids because they increase the reservoir permeability and thus influence oil/gas migration and production. If the fractures connect to a fault or Earth's surface, they will affect the migration, enrichment and preservation of oil/gas. Shale is a very tight rock with extremely low permeability but expresses good brittleness because of its organic-rich and fine-grained sediments[2]. Fortunately, generating a complex fracture network by hydraulic fracturing for oil/gas/water flowing in unconventional reservoirs is easier when the rock has a higher brittleness. When a large volume of fluid and other materials is injected into the targeted zones along vertical and/or horizontal wells, the injected fluid and other materials flow into pre-existing fractures and may result in slip, opening or closing of the pre-existing fractures and the development of new fractures, ultimately generating a more complex and more connected permeable network[3-5], creating new flow paths in the reservoir. Artificial fracture initiation and propagation are influenced by the following aspects. (1) Engineering operations, such as injection pressure, injection fluid viscosity and injection rate[6]. (2) Geological factors such as bedding planes, pre-existing fractures, fracture surface toughness, and regional tectonic stress. (3) Some geophysical factors, such as Young's modulus and brittleness, which affect and control the propagation of fracture networks[7], and the critical stress intensity[8] and pre-existing fractures, which contribute to fracture complexity[9].

During hydraulic fracturing, more than 70% of the influenced fractures slip, resulting from both fractured and faults[10,11]. Wei et al.[12] studied the rupture pattern of fractures and found that tension fractures are more easily developed near the well and that shear fractures tended to develop far from the well during coal fracturing. The fractures located by microseismic events (MEs) in the field or acoustic events (AEs) in the laboratory can reveal the temporal and spatial evolution and the spatial clustering characteristics of the fracture networks, especially the pre-existing fracture and fault damage zones. The differences in both the amplitude and dominant frequency of induced seismic waves also indicate the rupture scales of the fractures[13], which play different roles during hydraulic fracturing and oil/gas production.

(1) Large fractures/small faults may connect to hidden

faults and trigger small earthquakes, which may decrease oil/gas production and affect the lives of local residents[14-18]. (2) Medium-scale pre-existing fractures, fault damage zones or small faults may decrease the stimulated reservoir volume (SRV) and cause casing deformation and wellbore instability, which will hinder downhole tool operation and increase hydraulic fracturing expenses. The casing deformations in the Weiyuan-Changning block, southwest Sichuan Province, China, have close relationships with the small faults, fault damage and pre-existing fracture zones [19,20] and have resulted in more than 100 million yuan of additional engineering costs. These fracture and faulting zones are difficult to identify because they are beyond seismic resolution. Fracture or faulting zones predicted with 3D seismic data have shown an approximately 60% correlation to the casing deformation, and some casing deformations are related to hidden faults or other geological conditions. Additionally, pre-existing fractures/fault damage zones and small faults act as seepage channels of fracturing fluid and can result in small SRVs[21]. (3) Fracture networks provide important flow paths, storage and diffusion spaces for oil/gas/water[22]. The rupture scale, fracture geometry, rupture mechanism and accumulated SRV are crucial for planning reservoir exploitation and production and evaluating hydraulic fracturing[23], in which the connected fracture system provides a network of flow paths for gas diffusion and gas production.

Generally, four kinds of methods are used to study fracture development and propagation, including analytical calculations, numerical simulations, laboratory experiments [9] and field observations. An analytical method fits fractures with simplified planar shapes in a homogeneous isotropic medium [24]. A numerical simulation technique can be used to study the complex fracture behavior in a medium with pre-existing fractures, but the results depend on the accuracy of the numerical model, which represents the fracture complexity by simplification of the fracture geometry or assignment of structures such as pores, veins, and cracks as 3D geological attributes[25,26]. Laboratory experiments are an alternative method to simulate and observe the behaviors and mechanisms of fracture initiation and rupture processes in fractured and nonfractured reservoirs by simulating field conditions. This method is more effective in revealing the behaviors of complex fracture networks[27-29], and the recorded acoustic emission provides not only the temporal and spatial evolution but also the focal mechanism types of the ruptures, which can reveal the stress environment near the activated fractures[30,31]. Field observations can reflect the characteristics of fractures in real geological settings, but they have many uncertainties because of the complex geological environment and inaccessibility of underground zones. Microseismic monitoring is an important field technique and is widely used to reveal fracture behaviors under engineering operations. The temporal and spatial evolutions revealed by the located MEs are crucial data that can be used to reflect the SRV enhanced by hydraulic fracturing[32,33] and to research rupture behavior and fracture propagation. The conventional SRV is estimated by the density of MEs in a box of estimated height and area, and SRV can be equivalent to the 3D volume of the accumulated MEs. It is generally regarded that for a larger SRV, more oil/gas can be produced[34,35], but the real production may not follow this trend, and the probable reasons are as follows. One reason is the location error of MEs[36], which is necessary to improve the reliability of SRV estimation. The other is the detectability of MEs, which is related to the rupture scale of the activated fracture and the dissipation and attenuation of the seismic wave energy in the stratum. A larger rupture always triggers stronger ME, whereas one fracture within a network triggers weak ME[17], that is why seismic characteristics provide the possibility to characterize the rupture scale in the field. Acoustic emission is an effective method of revealing the microrupture characteristics of pores, bedding, cracks and microfractures, and microseismic monitoring is effective to demonstrate the characteristics of fracture networks, pre-existing fracture/fault damage zones and small faults in the field. Therefore, it is necessary to research rupture behavior at multiple scales by combining AEs in the laboratory and MEs in the field.

This paper studies the rupture mechanism and behavior of Longmaxi shale from the spatiotemporal evolution and distribution, focal mechanism and geometry of AEs in the laboratory and MEs in the field. The results indicate that shear slip dominates the rupture pattern. The ruptures tend to be activated along the multiscale fractures and pores, cracks, and bedding planes at the microscale to pre-existing fractures/fault damage zones and small faults at the macroscale. The pre-existing stress concentrations make rupture easier. The rupture behavior also accelerates the stress change at the fracture tip and results in a new stress concentration, which initiates and/or propagates ruptures via shear slip, opening/closing or collapse. The MEs detectability is related to the rupture scale, only the MEs with stronger energy releases, resulting from larger ruptures, can be detected and located. Because some MEs triggered by smaller ruptures are difficult to be effectively detect in the field, the zones without MEs are assumed to poor fracturing results, but this may not be the case, and the fracture networks in such areas greatly contribute to the SRV and oil/gas production over a long time.

2. Rupture Behavior in the Laboratory

Before engineering operations in the field, it is important to build a connection between the simulated experiments in the laboratory and engineering operations in the field by scaling laws[37]. Therefore, the fracture behaviors in the laboratory will more accurately reflect those in the field. The shale in this experiment comes from a geological outcrop of the Longmaxi Formation in the Changning block, southwest of the Sichuan Basin, China. The triaxial hydraulic fracturing experiment was operated and sensors were equipped to record the seismic wave radiated from the fracture activation. As shown in Figure 1, the simulated wellbore with a length of 533 mm was drilled from the top of the cuboid rock sample with a size of 762 mm×762 mm×941 mm, and the fracturing fluid was injected into the rock through the wellbore under triaxial confining pressure. The 24 channels of sensors were placed on the surfaces of the rock, and the rock was wrapped with cement to ensure its integrity during the experiment.

Approximately 300 detected and located AEs are shown in Figure 2. The activated fractures are mainly concentrated in the interior space near the wellbore and reflect the volumetric fractured zone.

The focal mechanism is the effect parameter to characterize rupture behavior. By using the moment tensor (MT) inversion method, the rupture pattern can be investigated by processing the AEs[38,39,40]. We use the waveform matching method of the P-wave to calculate the MT. If the correlation of the P-

wave between the observation and calculation reaches 0.8, a satisfying MT is produced. As shown in Figure 3, the beach balls are scaled by the averaged amplitude of the 24 channels and related to the rupture scale[13]. Clearly, the DC component dominates the rupture pattern, and some AEs have a few ISO and CLVD components, which indicate explosion, implosive or CLVD behavior and are probably accompanied by opening, closing or collapse of the tip of microfractures, bedding planes or cracks during the instant process of slip. The AEs with different rupture scales for each subfigure show the diversities of focal mechanisms, even at adjacent locations, and ruptures may mainly occur at pre-existing defects such as microfractures, bedding planes or cracks because pre-existing rupture surface is a prerequisite for DC behavior, and pre-existing microfractures, bedding planes or cracks are important weak surfaces in intact rock during hydraulic fracturing.

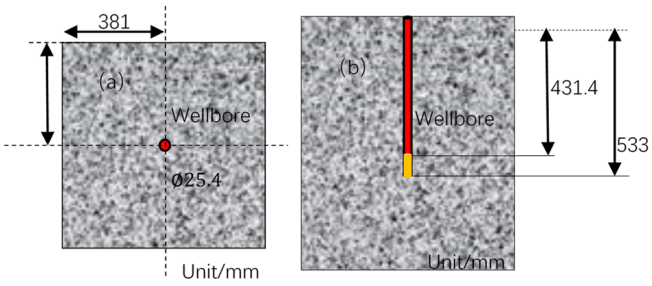


Figure 1. The rock sample diagram for the triaxial hydraulic fracturing experiment. (a)Top view of the rock sample, (b) side view of the rock sample. The red solid line in (b) is the simulated wellbore with a diameter of 25.4 mm, and the yellow part in (b) is the injection location for the liquid flowing into the rock.

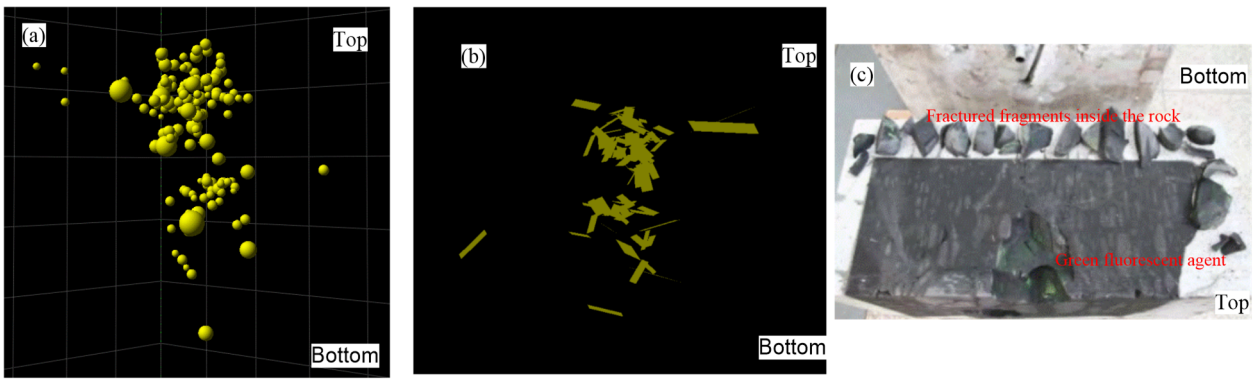


Figure 2. The activated fractures. (a) Located AEs in 3D, (b) the activated fractures with the focal mechanism successfully calculated and (c) the interior fragmentation of the broken rocks

The function $S(x, y, z, t, \phi_f, \delta, L, W)$ can be used to describe the geometry of activated fractures by simplifying the fractures to rectangular models. x, y and z represent the centroid coordinates of the fracture, and t is the rupture time. ϕ_f and δ are the orientation and dip of the fracture, respectively, and can be determined from the focal mechanism. L and W are the length and width of the evaluation rectangle and are closely related to the amplitude (scaled by the average ME amplitude), dominant frequency and duration of the wavelength [13], and the larger rupture scale, the stronger the amplitude and lower dominant frequency of the seismic wave, similar to the relationship between seismic waves and earthquakes. Some fractures in Figure 2(b), which may indicate that the fractures were activated along bedding. Some fractures are subvertical and connect bedding planes, and they may be microcracks or microfractures resulting from tectonic stress. The horizontal and vertical fractures connect to develop the fracture network and contribute to the SRV. The initial size and density of pre-existing defects, such as fractures, cracks or bedding planes, are the crucial factors that determine rock strength and govern the initial deformation damage. The normal stress on the fracture surface decreases with high-pressure fluid injection and decreases the friction on the surface; such processes accelerate the slip of the defect. Slip may be accompanied by opening, closing or collapse at the fracture tip during high-pressure fluid intrusion. The broken rocks in Figure 2(c) also indicate the diversities of rupture orientation and dip, which correspond to the fractures plotted in Figure 2(b). The green fluorescent agent in Figure 2(c) and the located AEs demonstrate that the injected fluid definitely contributes to the slippage. The AEs accumulate at a zone in the rock, and the green fluorescence shows that the injection fluid accumulated in the activated fractures within the rock.

3. Rupture Behavior in the Field

This case study focuses on the hydraulic fracturing of shale of the Longmaxi Formation, Sichuan Basin, China. The targeted shale is located at a depth of approximately 3,200 m, and many pre-existing fractures and fault damage zones or small faults have developed during multiple periods of tectonic activity, and they are easily reactivated during hydraulic fracturing, which releases considerable energy. In this case, the surface microseismic monitoring system with 10 receiving arms and 30 m spacing of adjacent stations was adopted to evaluate the hydraulic fracturing result, as shown in Figure 4.

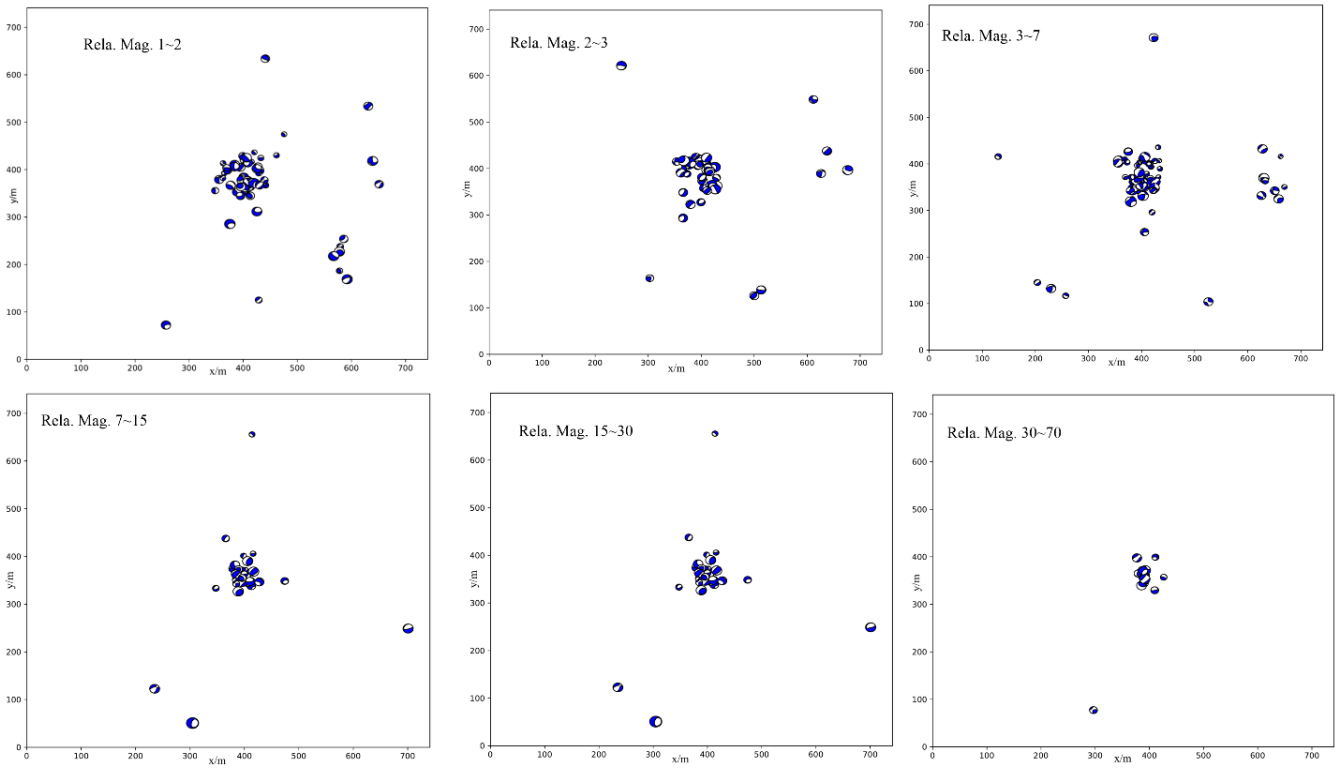


Figure 3. The focal mechanisms for different rupture scales for AEs. The beach ball is scaled by the averaged amplitude of the AEs for each subfigure

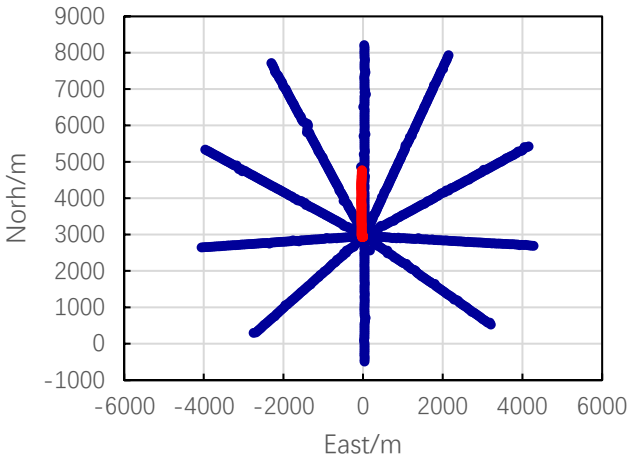


Figure 4. Top view of the microseismic monitoring system geometry. The blue curve indicates the 1-component geophones arranged on the surface, and the red solid line represents the treatment well.

As shown in Figure 5, more than 5,000 MEs were located near the wellbore and accumulate in three linear zones, as shown by the red solid lines in Figure 5(b). The MEs located in zones A, B and C show clustering features farther from the treatment well. Given that seismic characteristics, such as the amplitude, phase and duration, may reflect background noise and the rupture event, the location accuracy may be low because the Kirchhoff stacking method is used to automatically locate the Mes [41]; a quality control (QC) tool, such as 'Normal moveout', is needed to evaluate the location reliability [42]. By removing the time difference resulting from the propagation distance from the epicenter to the observation station, the arrival time of AEs for different observation stations should reflect a horizontal wave propagation. As Figure 6 shows, the P-wave for each receiving arm with strong and weak amplitudes generally remains horizontal after 'Normal moveout' processing; therefore, the located MEs in Figure 5 are reliable, and some MEs are located beyond the identified zones.

All located MEs in Figure 5 can be divided into three categories.

(1) Pre-existing fractures or fault damage zones near the wellbore. When faults or fault damage zones are developed, strong MEs can be triggered. The magnitude of such MEs is somewhat larger than that associated with MEs originating from fracture networks during fracturing operations because a larger surface area during slipping, opening, closing or collapse is available for rupture [14]. The distribution of the located MEs maintains the linear tendency indicated by the red solid lines in Figure 5(b), suggesting pre-existing clusters or fault damage zones, which easily reactivate during hydraulic fracturing[43,44]. The maximum horizontal

principal stress of the Longmaxi Formation shale in this block is 86-87 MPa in the east–west direction, the minimum horizontal principal stress is 71-73 MPa in the north–south direction, and the vertical principal stress is 82-85 MPa. The linearly distributed AEs almost maintain the same orientation of 45° clockwise from the north, and fault damage zones may have developed in the same tectonic setting.

(2) MEs were located far from the targeted zone but accumulated in the small clusters labeled A, B and C in Figure 5(b). We infer that such clusters also reflect pre-existing fracture or fault damage zone reactivation during hydraulic treatment. Because of the inelastic attenuation and energy propagation of seismic waves, some MEs were too weak to be detected and located, and only a few strong MEs were well detected and located. Because those MEs occurred beyond the coverage of the observation system, the location error in depth is much larger than that horizontally [45], as the zone circled by the red dotted line in Figure 5(a) shows.

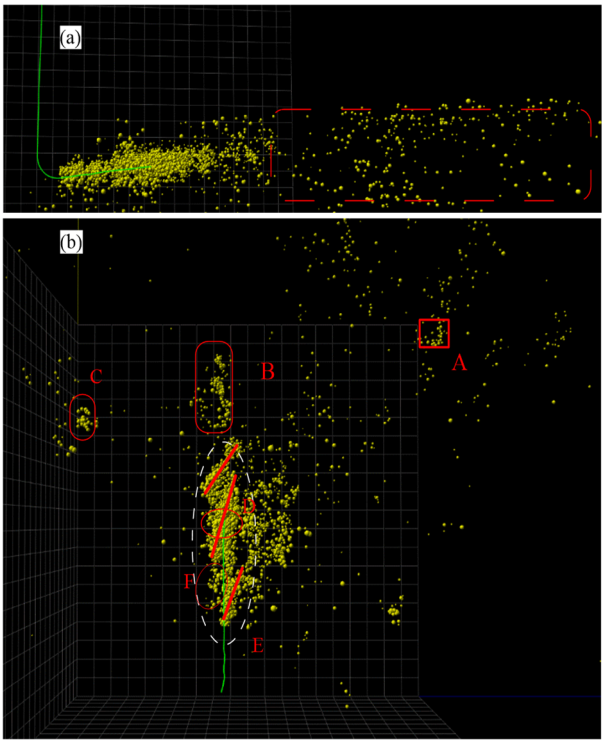


Figure 5. The located MEs. (a) Side view along the horizontal well, (b) top view. The grid size is 200 m×200 m, and the plotted MEs are scaled by the relative magnitude, which is related to the rupture scale; the larger the ball is, the larger the relative magnitude and rupture scale

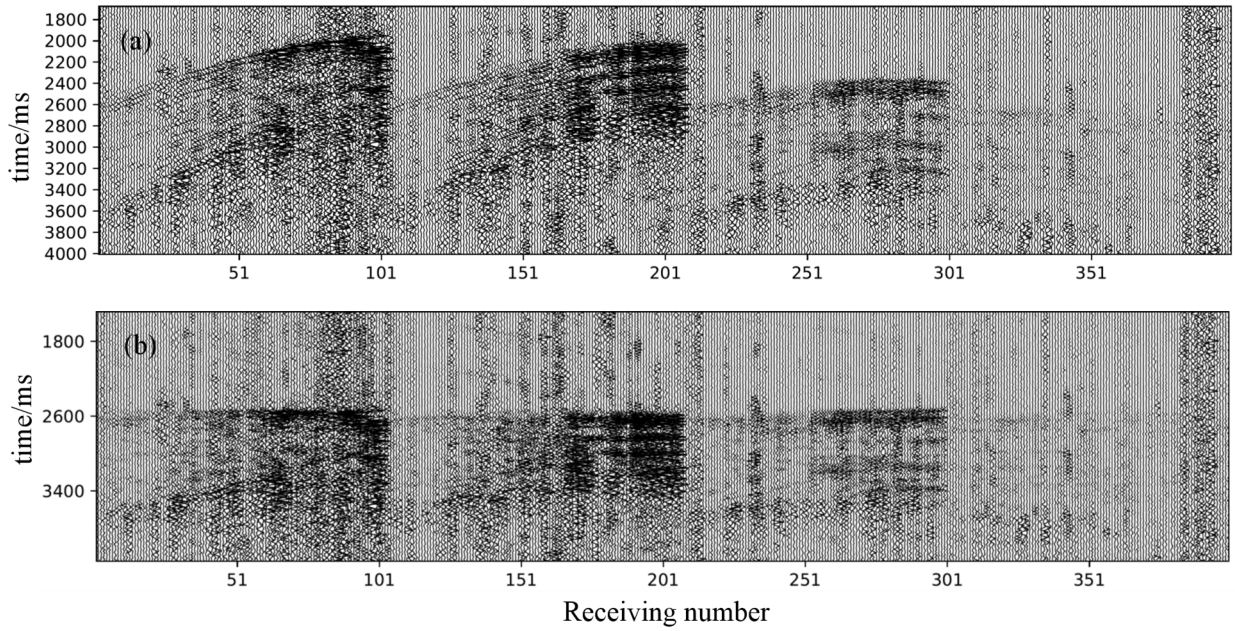


Figure 6. Microseismic wave located in zone A in Figure 5(b).
(a) and (b) are the microseismic wave before and after the 'Normal moveout' processing.

(3) The MEs near the wellbore. Many located MEs accumulated along the pre-existing fractures or fault damage zones[43,44], and it was difficult to differentiate and evaluate the fracture network, which greatly contributes to the estimated SRV and production performance. According to seismology theory [46], the seismic wave is composed of three parts, including the source time function $S(x_0, t)$, Green's function $G(x, t)$ and instrument response $R(x, t)$, as

shown in equation (1).

$$u(x,t) = S(x_0,t) * G(x,t) * R(f,\theta) \quad (1)$$

Different from earthquake observation method, with microseismic monitoring, the smaller receiving coverage and more focused epicenter location result in a shorter propagation distance in a similar stratum and with the same instrument response; thus, the effect of the Green's function $G(x,t)$ and instrument response $R(f,\theta)$ on MEs can be ignored. Therefore, the crucial factor resulting in the energy difference of MEs is the source time function[47], which characterizes the fracture scale and physical attributes of the rock, as equation (2) shows, where μ is the shear modulus and remains almost constant in the same reservoir and D is the displacement related to the size and shape of pre-existing fractures, bedding, cracks, etc. A is the rupture area and equals $L \times W$ when the fracture is simplified to be rectangular; usually, the larger A is, the wider D, and more energy release and stronger amplitudes are observed during MEs[45].

$$M_0 = \mu DA \quad (2)$$

Therefore, only a few MEs near the wellbore may indicate that a smaller rupture has developed, which makes the ME too weak to be effectively detected by the geophone or masked by ambient noise. In this case, because of the smaller fracture scale, it would be effective to accumulate energy/stress in the fractures, trigger slip to broaden and lengthen the fractures, and connect the other fractures to develop the fracture network, which is beneficial for the storage and flow of oil/gas/water and greatly contributes to the SRV and production [13].

The multiple orientations of the microseismic equipment are effective for obtaining the focal mechanism. We restricted the focal mechanism to the DC pattern to obtain the strike, dip and rake of the rupture because only the P-wave is reliably identified for most of the MEs. As Figure 7 shows, the focal mechanisms vary in different areas but also show similarities in adjacent zones.

There are four clusters of MEs that reflect pre-existing fractures or fault damage zones, labeled F1, F2, F3 and F4. The different relative magnitudes, in Figure 7(a)~(f), suggest a similar trend for F1, F2, F3 and F4, and they may have resulted from the same tectonic stress. The fault damage zone F1 has no contact with the treatment well, and we infer that the corresponding MEs were activated by stress interference. F2 is close to the treatment well; therefore, the factors that induced those pre-existing fractures to reactivate are more complex. This probably results from stress interference due to the pore pressure change and the interaction between the formation fluid and fracturing fluid.

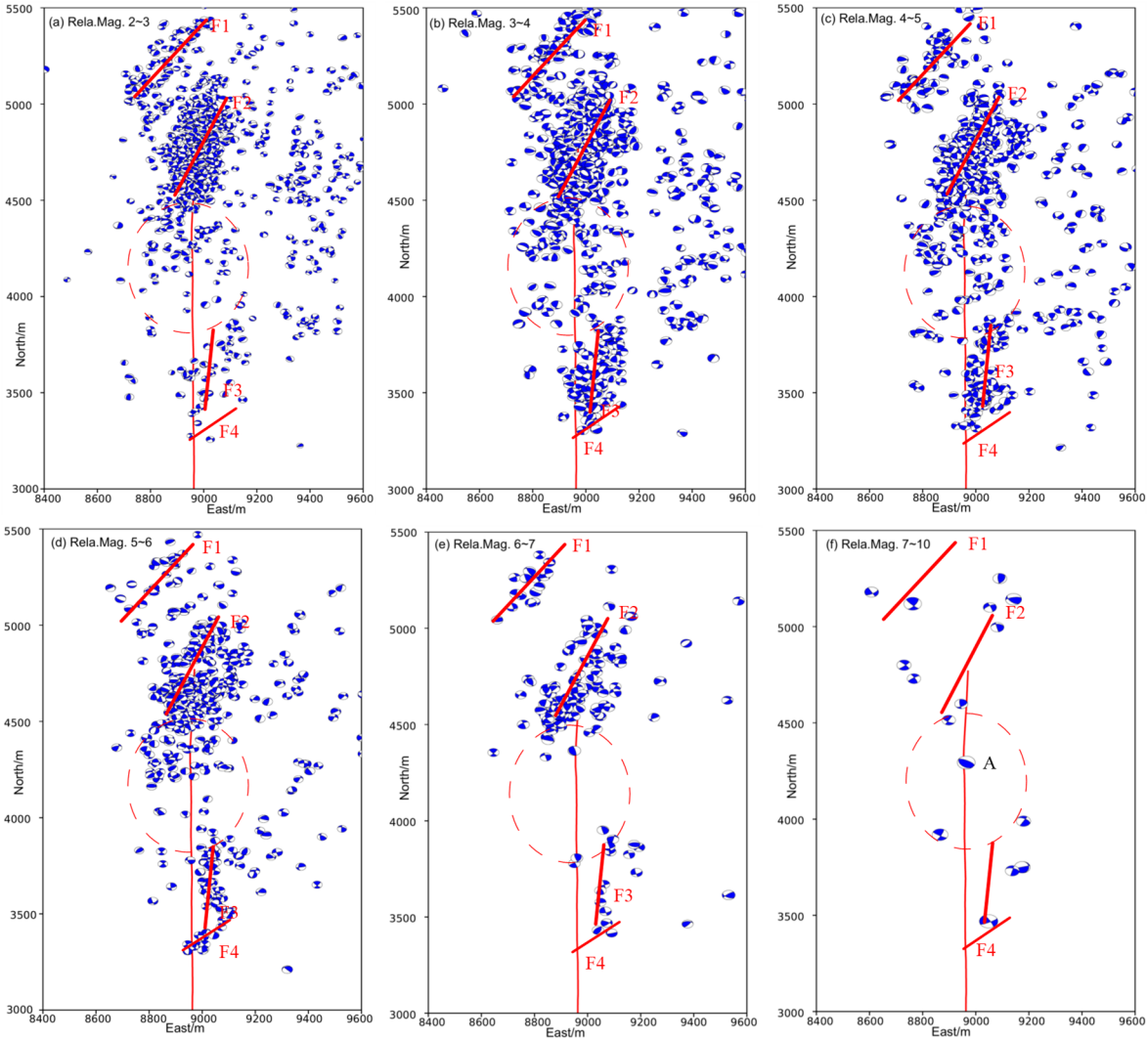


Figure 7. Focal mechanisms of MEs. The beach ball size is scaled by relative magnitude for each subfigure

The MEs with relative magnitudes of 2.0~6.0 in the red dotted elliptical zone reflect many new small fractures that developed and some scattered pre-existing fractures that reactivated during hydraulic fracturing and form the fracture

network[13]. However, the ME with a large relative magnitude at location A in Figure 7(f) is located adjacent to the treatment well and exhibits a reverse fault focal mechanism. Noticeably, there are no pre-existing fracture clusters or fault damage zones around A, and we infer a small hidden fault at A across the well trajectory. Pore pressure and fluid chemistry changes could potentially trigger shear slip on hidden faults with stress states near instability[48]. A larger fracture or fault surface is always accompanied by a larger displacement and aperture; therefore, larger pre-existing fractures or fault damage zones, or even small faults, can easily deform the well trajectory if they cross or are adjacent to the wellbore. Particularly, shear slip is common along pre-existing fractures, and the corresponding casing failure mechanism is shear deformation induced by fracture slip during hydraulic fracturing[20]. During hydraulic fracturing, the increased pore pressure decreases the effective stress on the fracture/fault surfaces, and the fracturing fluid decreases the friction on the fracture/fault surfaces, making it easier to trigger slip.

Combined with the geometry of the activated fractures characterized by the fracture definition function $S(x, y, z, t, \phi_f, \delta, L, W)$ in Figure 8, we classify the activated fractures into three categories. One is the fracture network in the red elliptical dotted zone; small fractures with multiple orientations develop the fracture network and can provide many flow paths for oil/gas/water during fracturing and later production. The second is pre-existing fractures or fault damage zones, labeled F1, F2, F3 and F4 in Figure 7, observable due to the MEs on reactivated fractures with multiple orientations and rupture scales. Such fractures result from multiple tectonic stress states and may be harmful to gas preservation. Meanwhile, the higher permeability in such areas may also result in leakage of the fracturing fluid and decrease the fracture development and SRV. The third is the small fault located at A in Figure 7; we infer that this is an small and isolated hidden fault with few large fractures connected to it. Because of its small length and surface area, it hardly results in fluid seepage during the fracturing operation, but it is dangerous for wellbore stability if reactivated.

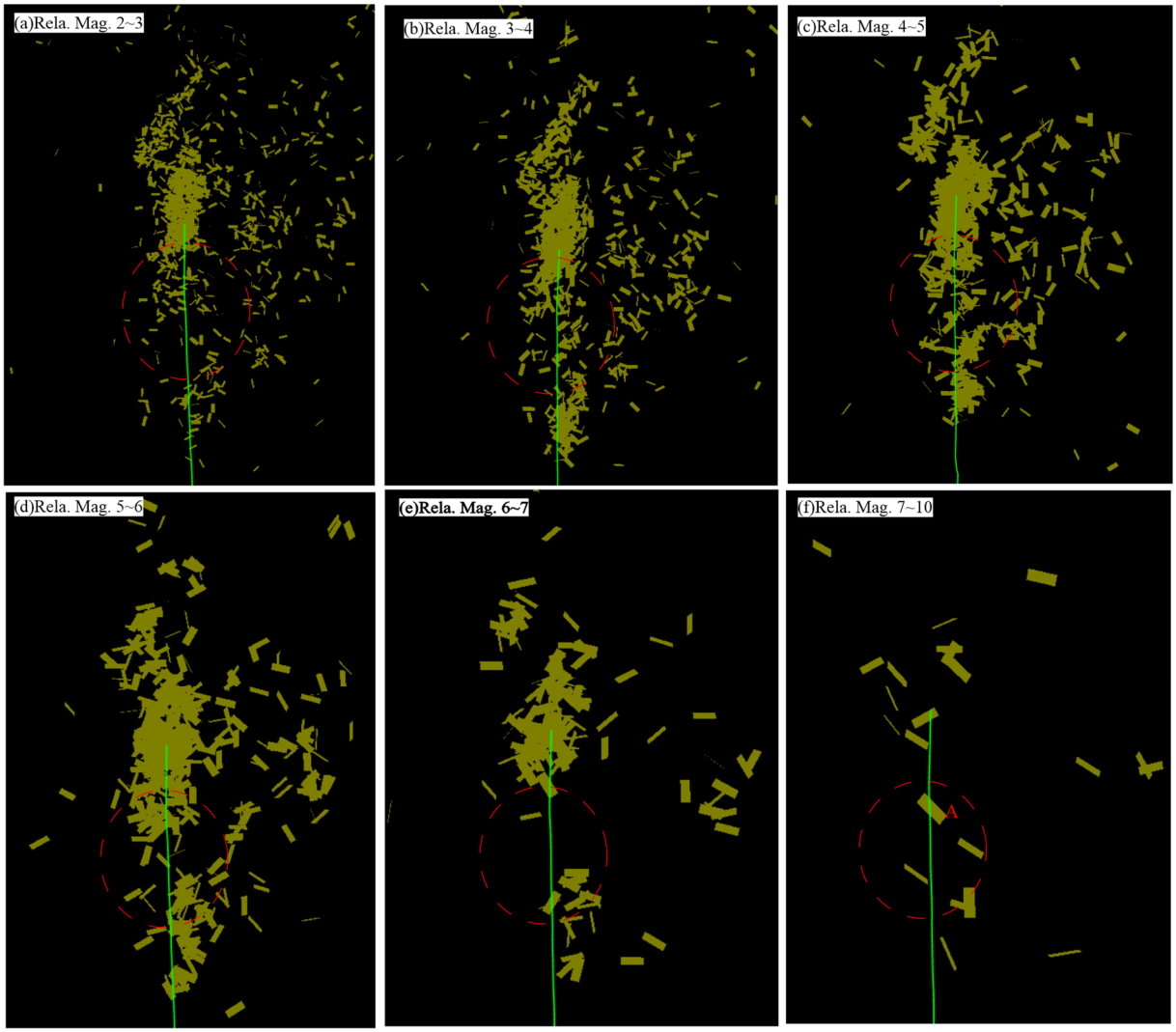


Figure 8. Geometry of activated fractures scaled by relative magnitude for each subfigure

4. Rupture Mechanism of Multiscale Fractures in Shale

Pre-existing fractures are important storage spaces and main seepage channels for oil/gas/water, and they also affect the rock permeability, migration, enrichment, preservation and production of oil/gas[49]. The shale of the Longmaxi Formation in the Sichuan Basin shows multiscale rupture features related to defects such as small faults, pre-existing fractures, fault damage zones, microfractures, cracks, bedding planes and pores. Therefore, the data reflect different

rupture patterns and characteristics at different scales during hydraulic fracturing. The AEs observed in the laboratory and MEs observed in the field suggest that the rupture patterns and characteristics of this shale have the following characteristics.

4.1. Multiscale Rupture Extension

Ruptures in the field usually develop during stress increases at defects such as microfractures, bedding planes, and pores. Different study objects rely on different hypotheses. If the study object is a tectonic earthquake with a large observation scale of hundreds to thousands of kilometers, the crust is simplified to several crucial homogeneous layers. For engineering scales such as hydraulic fracturing, the targeted zone is considered to be heterogeneous, and pre-existing fractures, fault damage zones, and small faults should be taken into consideration. The pores, veins/bedding planes, microfractures and cracks are equivalent to petrophysical properties such as Poisson's ratio and brittleness, but ambiguities arise when using brittleness to define the formation fragility, and the formation brittleness can be unrelated to the formation fragility[50]. Pores, veins, bedding planes, cracks and microfractures are important study objects in the laboratory. Multiscale defects, such as pores, veins, bedding planes, cracks, microfractures, pre-existing fractures/fault damage zones and small faults, can be independent but affect each other and contribute to the formation of multiscale fracture systems.

According to laboratory results, the AEs mainly stem from opening, closing[40] and slippage along fracture planes, and the shear component of the AEs was more sensitive to slip. Decreasing the shear strength and the effective stress or increasing the shear stress on fractures may trigger slip[51]. When external stress increases, the stress and strain increase at weak defects, such as pores, bedding planes, cracks and microfractures, to trigger rupture because of the lower compressive strength and shear strength of those defects. Therefore, the faults, pre-existing fractures and fault damage zones in rock easily trigger ruptures and open new seepage channels[14]. This is why MEs always accumulate at the pre-existing fracture and fault damage zones in the field, as in the four pre-existing fracture/fault damage zones shown in Figure 8.

The focal mechanism in the laboratory indicates that DC dominates the rupture pattern of the AEs. The diversities of the fracture and fragment geometry prove that pre-existing defects such as bedding planes, cracks and microfractures in rock are important prerequisites for slippage. The focal mechanism for some AEs involves both ISO and CLVD, which illustrates that the slippage on the fracture plane is also accompanied by an increase in pore pressure and a decrease in friction. The increasing pore pressure at the fracture tip and compressive stress resulting from the elastic strain during slip determine the opening, closing or collapse behavior at the fracture tip and eventually express the ISO and CLVD pattern.

4.2. SRV Evaluation

The rupture pattern is very important both for a single fracture and fracture network because the fracture size, geometry and connectivity are closely related to the rupture pattern and beneficial for fluid flow, seepage and oil/gas production. Notably, the rupture in Figure 2(c) probably begins along vein/bedding planes and microfractures, as the injected fluid seeps to such fracture surfaces and accelerates the slip by increasing the pore pressure and decreasing the friction on the surface. The slip on the fracture surface concentrates stress at the fracture tip and opens, closes or collapses under the compressive stress resulting from the elastic strain and pore pressure increase. Such interactions of slip on the fracture surface and tensile stress at the fracture tip make fractures reactivate and propagate, increasing the SRV.

Different from a microscale rupture in the laboratory, the located MEs in the field study accumulate along the pre-existing fractures and fault damage zones, and such MEs reflect a larger rupture scale[13] and usually hinder the development of the fracture network, probably for the following reasons.

(1) The larger rupture scale expresses a larger crack/fracture aperture, and fracturing fluid easily penetrates the fractures, resulting in seepage[30]. It is also difficult to accumulate stress and pore pressure to break through obstacles in a microfracture system to create new seepage channels and connect more rock to increase production performance.

(2) The pre-existing fractures and fault damage zones are the seepage channels for gas diffusion and are harmful to gas preservation in the long term. They provide seepage channels and accumulation space for oil/gas/water. If the fracture scale is too great, oil/gas/water may continue to seep and dissipate [52].

(3) The pre-existing fractures and fault damage zones may also contribute greatly to gas production in the short term if no fault connects to the surface. Pre-existing fractures always play a significant role in the initial stage of oil/gas production because they store free gas [52]. The accumulated gas in the pre-existing fractures and fault damage zone swill rapidly seep to the wellbore through the larger seepage channels of the pre-existing fractures and fault damage zones by high-speed non-Darcy flow, but it is difficult to maintain stable production since few microfractures are activated during hydraulic fracturing in this case, resulting in a less connected fracture network. Therefore, the SRV calculation should consider the role of pre-existing fractures and fault damage zones during hydraulic fracturing.

5. Discussion

This paper mainly focuses on the rupture characteristics of shale in the Sichuan Basin by combining AEs observed in the laboratory and MEs observed in the field. The propagation of fracture networks in the presence of pre-existing fractures is fundamentally different from fracture propagation in reservoirs without pre-existing fractures. Pre-existing fractures can significantly affect hydraulic fracturing behavior and production. This paper demonstrates that ruptures often occur on multiscale features such as pores, veins, bedding planes, cracks, microfractures, pre-existing fractures or small faults, which result in different strengths of the released seismic waves. The different rupture scales will trigger different strengths of seismic waves; therefore, some MEs triggered by smaller ruptures are difficult to effectively detect in the field, and those zones with a few MEs should be evaluated to reflect good fracturing results, which may indicate a fracture network that can greatly contribute to stable gas or oil production. The ME accumulation zones, which develop along pre-existing fractures and fault damage zones, should be classified into two types. One contributes to gas production in the short term because many larger complex fractures are activated and generate rapid gas flow in the related fractures and adjacent rock. These zones have

difficulty supporting stable production in the long term because the leakage of the fracturing fluid makes it difficult for the fracturing fluid to penetrate microfractures and produce slippage to widen fractures and connect more zones in the rock. The other also probably indicates poor gas production because the fractures may connect to the surface or other formations and gas may be dissipated.

However, weak signals may represent the areas without pre-existing or new fractures and thus will contribute poorly to production. Therefore, fracturing evaluation with MEs should combine the following considerations. (1) Temporal and spatial evolutions and distribution. The ME clusters and some specific ME-triggered zones are labeled by the red dashed elliptical area in Figure 5 and correspond to the AEs in Figure 2. (2) The geological setting, such as the brittleness, pre-existing fracture and small fault distributions, stress and heterogeneity determined from seismic and logging data. (3) The engineering operation and related pumping data. The pumping curve is also a comprehensive reflection of the reservoir physics, as Figure 2 shows from the laboratory work.

Regarding whether fracture activation is triggered by stress perturbation or fluid pressure, we consider two aspects. The fractures in networks seem to be more easily activated by pore pressure changes related to fluid injection and extraction. Therefore, the MEs or AEs corresponding to fracture networks may indicate the area where the fracturing fluid is, as the broken rock and fluorescence in Figure 2 coincide with the AE locations. The second concerns the stress perturbation near pre-existing fractures or fault damage areas, as shown by the MEs in the field in Figures 8. The increasing or decreasing stress changes the original stress setting, and stress perturbation at fracture surfaces can reactivate the fractures.

6. Conclusion

AEs and MEs are effective observations that can be analyzed to reveal the changes in rock because they not only provide the temporal and spatial evolution and detailed characteristics of rupture but also reveal the mechanism of the rupture initiation and propagation and relative rupture scales. Hydraulic evaluation is a complex and compound process, and the characteristics of multiscale rupture increase this complexity. From the microscale to the macroscale, the ruptures that occur during the hydraulic fracturing of shale show a DC pattern predominantly, with some ISO and CLVD. Therefore, the rupture pattern for hydraulic fracturing generally remains the same for the multiscale objects studied. However, they may also express the different temporal and spatial evolution and distribution characteristics of features such as pores, cracks, veins, and bedding planes in the laboratory and network fracture systems and pre-existing fracture or fault damage zones in the field, even among different geological settings. Such multiscale rupture behaviors combined with the original geological setting result in engineering problems and make hydraulic fracturing evaluation challenging.

Therefore, it is necessary to use acoustic emission systems in the laboratory and microseimic monitoring systems in the field.

(1) Laboratory tests are a visible tool that can be used to research petrophysical attributes and simulate the response of fracturing materials and operations on rock by providing deterministic results, such as the visible distribution of fracturing fluid and activated fractures. The acoustic emission provides data for determining not only a temporal and spatial evaluation process of activated fractures but also the rupture pattern, relative rupture scale, and accurate focal mechanisms. In addition, acoustic emission is similar to microseismic monitoring and is crucial for developing the relationship among the multiple scales of fractures. The combination of acoustic emission and microseismic monitoring is helpful to understand the underground environment.

(2) Microseismic monitoring is an important tool to evaluate hydraulic fracturing, similar to a borehole videography in the formation, microseismic monitoring can record the temporal and spatial changes in ruptures. It reflects the time, location, rupture pattern, scale and geometry of the ruptures to reveal the rock behavior during hydraulic fracturing. The accuracy of the epicenter location is extremely important; therefore, QC tools are necessary to evaluate the reliability of this approach. Due to the influence of wave propagation distance and rupture scale, some MEs are difficult to effectively detect. Zones with a few or no MEs represent poor contributions to production, and zones with many MEs represent good contributions. It is necessary to comprehensively evaluate the effectiveness and SRV by combining the ME results, local geological characteristics, hydraulic treatment curves, 3D seismic data, petrophysical attributes and laboratory data.

(3) With the long-term and multistage tectonic activity around the Sichuan Basin, pre-existing fractures, fault damage zones and small faults are well developed in the shale of the Weiyuan-Changning block. Compared to new fractures, these pre-existing fractures are more likely to cause wellbore deformation [19]. Therefore, during hydraulic fracturing in this area, it is crucial to closely monitor the fracture rupture and propagation caused by the pre-existing fracture or fault damage zones and small hidden faults.

(4) In either the laboratory or field, the pores, bedding planes, veins, cracks and fractures have the potential to reactivate at different scales. There are always many pores, veins, bedding planes, cracks and microfractures in the field, but too weak of a seismic wave may be released to be detected and located, which causes such features to be overlooked.

Acknowledgments

The paper was supported by the projects ‘Research on Artificial Fracture Network Characterization and Geomechanical Parameters by Microseismic monitoring in the year 2023-2024’ (Project No. XNS JS2023-50) and ‘Study on the mechanism of fracture initiation/extension based on epicenter parameters of activated microfractures for tight reservoirs’ (Project No. SKLGME022006).

References

[1] Lefèvre, M., Guglielmi, Y., Henry, Dick, P., & Gout, C., 2016. Calcite veins as an indicator of fracture dilatancy and connectivity during strike-slip faulting in Toarcian shale (Tournemire tunnel, Southern France), J Struct Geol, 83,73-84.

[2] Javadpour, F., Fisher, D., & Unsworth, M., 2007. Nanoscale gas flow in shale gas sediments, J.Can.Pet.Technol., 46 (10), 55-61.

[3] Jahandideh, A., & Jafarpour, B., 2016. Optimization of hydraulic fracturing design underspatially variable shale fracability, J.Pet.Sci.Eng.,138, 174-188.

[4] Zhang, D., Ranjith, P.G., & Perera, M.S.A., 2016. The brittleness indices used in rock mechanics and their application

in shale hydraulic fracturing: a review, J. Pet. Sci. Eng.,143, 158–170.

[5] Kivi, I. R., Ameri, M., & Molladavoodi H., 2018. An experimental investigation on deformation and failure behavior of carbonaceous Garau shale in Lurestan Basin, west Iran: Application in shale gas development, J Nat Gas Sci Eng, 55,135-153.

[6] Dutler, N., Nejati, M., Valleya, B., Amannc, F., & Molinari, G., 2018. On the link between fracture toughness, tensile strength, and fracture process zone in anisotropic rocks, Eng Fract Mech, 201,56-79.

[7] Figueiredo, B., Tsang, C. F., Rutqvist, J., & Niemi, A., 2017. Study of hydraulic fracturing processes in shale formations with complex geological settings, J.Pet.Sci.Eng., 152, 361-374.

[8] Mutlu, O., & Bobet, A., 2005. Slip initiation on frictional fractures, Eng Fract Mech, 72(5), 729-747.

[9] Dehghan, A. N., 2020. An experimental investigation into the influence of pre-existing natural fracture on the behavior and length of propagating hydraulic fracture, Eng Fract Mech, 240, 107330.

[10] Shan, K., Zhang, Y., Zheng, Y., Cheng, Y., & Yang, Y., 2021. Effect of fault distribution on hydraulic fracturing: Insights from the laboratory, Renew.Energ., 163, 1817-1830.

[11] Zhong, J., Liu, S., Ma, Y., Yin, C., Liu, C., Li, Z., Liu, X., & Li, Y., 2015. Macro-fracture mode and micro-fracture mechanism of shale. Pet. Explor. Dev., 42(2), 269-276.

[12] Wei, H., Li, L., Wu, X., & Hu, Y., 2011. The Analysis and Theory Research on the Factor of Multiple Fractures During Hydraulic Fracturing of CBM Wells, Prog. Earth Planet. Sci., 3, 231-237.

[13] Yin C., 2017. Fault detection based on microseismic events, Appl. Geophys., 14(3), 363-371.

[14] Rutqvist, J., Rinaldi, A. P., Cappa, F., & Moridis, G. J., 2015. Modeling of Fault Reactivation and Induced Seismicity During Hydraulic Fracturing of Shale-Gas Reservoirs, J.Pet.Sci.Eng., 127, 377-386.

[15] Lei, X., Huang, D., Su, J., Jiang, G., Wang, X., Wang, H., Guo, X., & Fu, H., 2017. Fault reactivation and earthquakes with magnitudes of up to Mw4.7 induced by shale gas hydraulic fracturing in Sichuan Basin, China, Sci.Rep., 7, 7971.

[16] Zoback, M.D., & Gorelick, S.M., 2012. Earthquake triggering and large-scale geologic storage of carbon dioxide, P.Natl.Acad.Sci.USA, 109(26), 10164-10168.

[17] Ellsworth, W. L., 2013. Injection-induced earthquakes, Science, 341, 1225942.

[18] Lei, X., Ma, S., Chen, W., Pang, C., Zeng, J., & Jiang, B., 2013. A detailed view of the injection-induced seismicity in a natural gas reservoir in Zigong, southwestern Sichuan Basin China, J.Geophys.Res.Solid Earth, 118(8), 4296-4311.

[19] Chen, Z., Shi, L. & Xiang, D., 2017. Mechanism of casing deformation in the Changning-Weiyuan national shale gas project demonstration area and countermeasures, Natural gas industry B, 6(1), 1-6.

[20] Yin, F., Xiao, Y., Han, Li., & Wu, X., 2018. Quantifying the induced fracture slip and casing deformation in hydraulically fracturing shale gas wells, J Nat Gas Sci Eng, 60, 103-111.

[21] Wu, S., Ge, H., Wang, X., & Meng, F., 2017. Shale Failure Processes and Spatial Distribution of Fractures Obtained by AE Monitoring, J Nat Gas Sci Eng, 41,82-89.

[22] Rutledge, J., Phillips, W. S. & Mayerhofer, M. J., 2004. Faulting Induced by Forced Fluid Injection and Fluid Flow Forced by Faulting: An Interpretation of Hydraulic-Fracture Microseismicity, Carthage Cotton Valley Gas Field, Texas, Bull.Seismol.Soc.Am., 94(5), 1817-1830.

[23] Shao,Y., Huang, X., & Xing, Y., 2017. An integrated study on the sensitivity and uncertainty associated with the evaluation of stimulated reservoir volume (SRV), J.Pet.Sci.Eng., 159, 903-914.

[24] Dehghan, A. N., Goshtasbi, K., Ahangari, K., Jin, Y., & Bahmani, A., 2017. 3D numerical modeling of the propagation of hydraulic fracture at its intersection with natural (pre-existing) fracture, Rock Mech Rock Eng, 50, 367-386.

[25] Tan, P., Jin, Y., Han, K., Hou, B., Chen, M., Guo, X., Guo, X., & Gao, J., 2017. Analysis of hydraulic fracture initiation and vertical propagation behavior in laminated shale formation, Fuel, 206, 482-493.

[26] Hou, B., Zhang, R., Zeng, Y., Fu, W., Muhadasi, Y., & Chen, M., 2018. Analysis of hydraulic fracture initiation and propagation in deep shale formation with high horizontal stress difference. J.Pet.Sci.Eng., 170, 231-243.

[27] Chen, P., Han Q., Ma T., & Lin D., 2015. The mechanical properties of shale based on micro-indentation test, Pet.Explor.Dev., 42(5), 723–732.

[28] Dehghan, A. N., Goshtasbi, K., Ahangari K., & Jin, Y., 2015. Mechanism of fracture initiation and propagation using a tri-axial hydraulic fracturing test system in naturally fractured reservoirs, Eur.J.Environ, 20(5), 560-585.

[29] Tan, P., Pang, H., Zhang, R., Jin, Y., Zhou, Y., Kao, J., & Fan, M., 2020. Experimental investigation into hydraulic fracture geometry and proppant migration characteristics for southeastern Sichuan deep shale reservoirs, J.Pet.Sci.Eng., 184, 106517.

[30] Wu F., Yan Y., Yin C., 2016. Real-time microseismic monitoring technology for hydraulic fracturing in shale gas reservoirs: A case study from the Southern Sichuan Basin. Natural gas industry, 36(11), 46-50.

[31] Cebry, S. B. L.& McLaskey, G. C., 2021. Seismic swarms produced by rapid fluid injection into a low permeability laboratory fault, Earth Planet.Sci.Lett., 557, 116726.

[32] Ouenes, A., Nicholas, M. U., & Aimene, Y. E., 2016. Using geomechanical modeling to quantify the impact of natural fractures on well performance and microseismicity: application to the wolfcamp, permian basin, reagan county, texas. Interpretation, 4(2), SE1-SE15.

[33] Rogers, S., 2003. Critical stress-related permeability in fractured rocks. Geological Society London Special Publications, 209(1), 7-16.

[34] Xu, J., Guo, C., Teng, W., Wei, M., & Jiang, R., 2015a. Production performance analysis of tight oil/gas reservoirs considering stimulated reservoir volume using elliptical flow. J Nat Gas Sci Eng, 26, 827-839.

[35] Xu, J., Guo, C., Wei, M., & Jiang, R., 2015b. Production performance analysis for composite shale gas reservoir considering multiple transport mechanisms. J Nat Gas Sci Eng, 26, 382-395.

[36] Yong, Y. K., Maulianda,M., Wee, S. C., Mohshim, D., Elraies, K. A., Wong, R. CK., Gates, I. D., & Eaton, D., 2018. Determination of stimulated reservoir volume and anisotropic permeability using analytical modelling of microseismic and hydraulic fracturing parameters, J Nat Gas Sci Eng, 58, 234-240.

[37] Li, X., Lei, X., Li, Q., & Chen, D., 2021. Influence of bedding structure on stress-induced elastic wave anisotropy in tight sandstones, Journal of Rock Mechanics and Geotechnical Engineering, 13(1), 98-113.

[38] Lei, X., Nishizawa, O., & Satoh, T., 1992. Fractal Structure of the Hypocenter Distributions and Focal Mechanism Solutions of Acoustic Emission in Two Granites of Different Grain Sizes, Journal of Physics of the Earth, 40(6), 617-634.

[39] Sellers, E. J., Kataka, M. O., & Linzer, L. M., 2003. Source parameters of acoustic emission events and scaling with miningüinduced seismicity, J.Geophys.Res.Solid Earth, 108(B9), B000670.

[40] Zhai, H., Chang, X., Wang, Y., Lei, X., & Xue, Z., 2020. Analysis of acoustic emission events induced during stress unloading of a hydraulic fractured Longmaxi shale sample, J. Pet. Sci. Eng., 189,106990.

[41] Liang, C., Yu, Y., Yang, Y., Kang, L., Yin, C., & Wu, F., 2016. Joint inversion of source location and focal mechanism of microseismicity,

[42] Geophysics, 81(2), KS103-KS111. Castle, R. J., 1994. A theory of normal moveout, Geophysics, 59(6), 983-999.

[43] Gudmundsson, A., 2004. Effects of Young's modulus on fault displacement, CR GEOSCI, 336(1), 85-92.

[44] Chen, H., Meng, X., Niu, F., Tang, Y., Yin, C., & Wu, F., 2018. Microseismic monitoring of stimulating shale gas reservoir in SW China: 2. Spatial clustering controlled by the preexisting faults and fractures, J.Geophys.Res. Solid Earth, 123, 1659–1672.

[45] Yin, C., 2017. The research and application of rupture characteristic for microseismic epicenter , Ph.D. thesis, Chengdu University of Technology.

[46] Seth, S., & Michael, W., 2002. An introduction to seismology, earthquakes and earth structure, Britain: Blackwell Publishing.

[47] Zhang, Y., 2008. Study on the Inversion Methods of source rupture process, Ph.D. thesis, Peking University.

[48] Barbour, A. J., 2015. Pore pressure sensitivities to dynamic strains: observations in active tectonic regions, J. Geophys. Res. Solid Earth., 120(8), 5863-5883.

[49] Gu, Y., Ding, W., Tian, Q., Xu, S., Zhang, W., Zhang, B., & Jiao, B., 2020. Developmental characteristics and dominant factors of natural fractures in lower Silurian marine organic-rich shale reservoirs: A case study of the Longmaxi formation in the Fenggang block, southern China, J.Pet.Sci.Eng., 192, 107277.

[50] Bai, M., 2016. Why are brittleness and fracability not equivalent in designing hydraulic fracturing in tight shale gas reservoirs, Petroleum, 2(1), 1-19.

[51] Rutqvist J., Graupner, B., Guglielmi, Y., Kim, T., Maßmann, J., Nguyen, T. S., Park, J. W., Shiu, W., Urpi, L., Yoon, J. S., Ziefle, G., & Birkholzer, J., 2020. An international model comparison study of controlled fault activation experiments in argillaceous claystone at the Mont Terri Laboratory, Int.J.Rock.Mech.Min., 136, 104505.

[52] Ding, W. L., Li, C., Li, C. Y., Xu, C. C., Jiu, K., Zeng, W. T., & Wu, L. M., 2012. Fracture development in shale and its relationship to gas accumulation. Geosci. Front., 3(1), 97-105.